Research Square

Preprints are preliminary reports that have not undergone peer review.
They should not be considered conclusive, used to inform clinical practice,
or referenced by the media as validated information.

Distinct adipocyte size profiles and progenitor cell signatures underlie orbital adipose tissue expansion in Graves' orbitopathy

Pauline Decaunes
INSERM/Toulouse University
Pénélope Viana
INSERM/Toulouse University
Jean Galitzky
INSERM/Toulouse University
Benoit Chaput
Toulouse University Hospital
Solange Grunenwald
Toulouse University Hospital
Philippe Imbert
Toulouse University Hospital
Céline Dekeister
Toulouse University Hospital
Anne Bouloumié
INSERM/Toulouse University
Philippe Caron
caron.p@chu-toulouse.fr

INSERM/Toulouse University

Research Article

Keywords: Thyroid eye disease, subcutaneous adipose tissue, hyperplasia, hypertrophy, adipogenesis

Posted Date: November 16th, 2026

DOI: https://doi.org/10.21203/rs.3.rs-11161746/v1

License: This work is licensed under a Creative Commons Attribution 4.0 International License.
Read Full License

Additional Declarations: No competing interests reported.

Distinct adipocyte size profiles and progenitor cell signatures underlie orbital adipose tissue expansion in Graves' orbitopathy

Pauline Decaunes[1] ; Pénélope Viana[1] ; Jean Galitzky[1] ; Benoit Chaput[2]; Solange Grunenwald[3] ; Philippe Imbert[3, 4]; Céline Dekeister[3]; Anne Bouloumié*[1]; Philippe Caron*[1,3]

* equally contributed

[1] Institute of Metabolic and Cardiovascular diseases, INSERM/Toulouse University, UMR1297, Toulouse, France;

[2] Department of Plastic and Reconstructive Surgery, Rangueil, Toulouse University Hospital, France;

[3] Multidisciplinary orbitopathy consultation, Endocrinology and Metabolic Diseases Department, Cardiovascular and Metabolic Pole, Larrey, Toulouse University Hospital, France;

[4] Ramsay- Clinique La Croix du Sud, Quint-Fonsegrives, France

Keywords: Thyroid eye disease, subcutaneous adipose tissue, hyperplasia, hypertrophy, adipogenesis

Conflict of interest statement: The authors have declared that no conflict of interest exists.

Short title: Orbital progenitor heterogeneity in Graves' orbitopathy.

Abstract

Background: Graves' orbitopathy (GO) is characterized by expansion of orbital adipose tissue (OAT), causing proptosis and, in severe cases, compressive optic neuropathy. However, the adipocyte size profile and adipose progenitor cell (APC) heterogeneity underlying depot-specific OAT expansion remain poorly defined.

Methods: We compared adipocyte morphology and APCs ($CD45^{-}CD31^{-}CD34^{+}$ cells) in OAT from patients with GO (n = 33) and abdominal subcutaneous adipose tissue (SAT) from controls without GO (n = 10–17). APC subsets were characterized by flow cytometry using CD31, CD55, CD36, CD271, and MSCA1. Within the GO cohort, adipocyte size and progenitor subsets were related to demographic and clinical measures (EUGOGO classification, clinical activity score, TSH-receptor antibody (TRAb) status, Hertel exophthalmometry and Gorman diplopia score) using unsupervised clustering and stratification.

Results: OAT adipocytes were significantly smaller than abdominal SAT adipocytes. The APC fraction was reduced in OAT, with lower expression of CD34, CD36, MSCA1, and CD271, but increased CD55 positivity compared with SAT. Adipocyte size and SVF composition identified distinct demographic and clinical patterns. Larger adipocytes were associated with older age whereas smaller adipocytes were linked to greater disease activity/severity and TRAb positivity. A cell cluster enriched in $CD55^{+}$ progenitor subset was associated with greater proptosis (Hertel $\geq$ 23 mm).

Conclusions: GO OAT displays a distinct adipocyte and progenitor phenotype. A CD55-enriched, CD36/MSCA1-low progenitor subset is associated with clinical proptosis while smaller adipocytes characterize more active/severe disease, suggesting hyperplastic OAT expansion during active GO and a shift toward hypertrophy with aging and inactive GO. These

findings identify $CD55^{+}$ orbital APCs as potential contributors to GO pathogenesis and candidate biomarkers or therapeutic targets.

Corresponding author: Philippe Caron

The Email Address of the Corresponding Author is caron.p@chu-toulouse.fr

This research did not receive any specific funding.

Introduction

Graves' orbitopathy (GO) is the most common extrathyroidal manifestation of Graves' disease and represents a major cause of acquired diplopia and disfiguring proptosis in adults [1]. GO is driven by autoimmune activation of orbital stromal cells, which respond to TSH-receptor autoantibody (TRAb) signaling with excess hyaluronan production, myofibroblast differentiation, and expansion of orbital adipose tissue (OAT) [2]. Because the bony orbit is a rigid, non-distensible compartment, even modest volumetric expansion of OAT translates into thyroid eye disease (TED) with proptosis, extraocular muscle restriction, and, in severe cases, orbital crowding and sight-threatening disease [1]. Since classical adipose depots are generally depleted during the hypermetabolic state of untreated Graves' disease, the cellular basis that distinguishes orbital adipose tissue from conventional metabolic fat depots remains incompletely defined.

Orbital fat represents a particularly unique fat depot. Unlike most adipose depots, orbital adipose tissue has a predominantly neural crest developmental origin [3],[4] and fulfills specialized anatomical functions within the orbit. Rather than serving primarily as an energy-storage depot, orbital adipose tissue provides mechanical support to the intraorbital structures and facilitates their movement. Consistent with this specialized role, orbital fat appears to be less influenced by obesity than classical white adipose tissue [5]. In addition, OAT has a distinctive adipocyte biology. Experimental studies suggest that orbital fat may possess brown-like characteristics [3]. OAT adipocytes are smaller than subcutaneous or visceral adipocytes, show low lipolytic activity and appear to expand predominantly through hyperplasia rather than through the hypertrophic expansion seen in other depots [6],[7]. This raises the possibility that the adipose progenitor cells (APCs) that give rise to orbital adipocytes are themselves functionally distinct from APCs in more extensively studied depots such as abdominal subcutaneous adipose tissue (SAT).

In humans, APCs are classically identified within the stromal vascular fraction (SVF) as $CD45^{-}$ $CD31^{-}CD34+$ [8]. Importantly, the phenotype of native human APCs differs substantially from that of cultured adipose-derived stromal cells (ASCs), which progressively lose CD34 and acquire a classical mesenchymal stromal phenotype (CD73+CD90+) [9]. Increasing evidence indicates that human APCs are themselves highly heterogeneous. Multiparameter flow cytometry and single-cell transcriptomic approaches have identified several phenotypically and functionally distinct progenitor populations within human adipose tissue. CD55, often studied jointly with DPP4 and PI16 in single-cell transcriptomic atlases of human fat, marks a more quiescent, multipotent, upstream progenitor state from which both adipogenic and non-adipogenic lineages arise [10-12]. CD36 marks a subset with pronounced adipogenic and triglyceride-storage capacity [13], while MSCA1 (alkaline phosphatase, ALPL) and CD271 (NGFR) further stratify progenitors according to their spatial niche and lineage, with $MSCA1^{+}$ cells enriched in the adipogenic stroma and CD271-high cells enriched in fibrous septa and biased toward a myofibroblastic fate [14]. Whether this progenitor hierarchy, established primarily in SAT and visceral depots, is conserved in OAT, and whether specific progenitor subsets are associated with the degree of adipose expansion and clinical severity in GO, has not been systematically examined.

In the present study, we compared mature adipocyte morphology and SVF cellular composition in OAT from patients with GO and abdominal SAT from controls. We first quantified adipocyte diameter and examined the distribution of adipocyte sizes rather than relying solely on mean diameter. We then characterized CD45/CD34-defined SVF populations and further resolved the $CD45^{-}CD34^{+}CD31^{-}$ progenitor compartment using CD55, CD271, CD36, and MSCA1. Finally, we investigated whether adipocyte morphology and progenitor-cell subsets were associated with clinical measures of TED activity and severity within the GO cohort.

Materials and Methods

Tissue Collection

The study protocol was approved by the Ministère de la Recherche, Direction Générale de la Recherche et de l'Innovation, Cellule Bioéthique (DC2008-452), in accordance with ethical standards. All participants provided written informed consent after receiving an explanation of the purposes of the study. Clinical characteristics of patients with GO are presented in Table 1.

All patients undergoing orbital surgery underwent bony orbital decompression performed by the same surgeon (D.C.). Indications for surgery were based on disease severity and activity. Seven patients with sight-threatening GO, classified according to the European Group on Graves' Orbitopathy (EUGOGO) criteria, were treated with 2 or 3 intravenous pulse doses of methylprednisolone administered every 1 or 2 days. Five patients who did not respond to corticosteroid treatment subsequently underwent urgent bony orbital decompression. During the inactive phase of GO, orbital decompression was performed to improve visual function and aesthetic appearance in patients with significant or disfiguring proptosis.

Abdominal subcutaneous adipose tissue was obtained from 17 lean women participating in the GLUTAB cohort (ClinicalTrials.gov identifier NCT01605578) for adipocyte-size distribution analyses. These participants had a mean age of 34 years (range, 25–44 years) and a mean BMI of 24.8 kg/m² (range, 21.4–27.5 kg/m²). For flow-cytometric analyses, abdominal subcutaneous adipose tissue was obtained from 10 donors (9 women and 1 man) undergoing elective dermolipectomy. These donors had a mean age of 43 years (range, 35–58 years) and a mean BMI of 27.0 kg/m² (range, 19.7–31.9 kg/m²).

Adipose Tissue Digestion and Isolation of Mature Adipocytes and Stromal Cells

Adipose tissue cells were isolated and analysed as previously reported [14]. Briefly, orbital and abdominal subcutaneous adipose tissues were weighed and digested with type I collagenase

(250 U/mL; Sigma-Aldrich). Following digestion and centrifugation, the upper phase containing mature adipocytes and the pellet containing the stroma-vascular cells (SVF) were collected. After washing steps, mature adipocytes were photographed by phase-contrast microscopy and adipocyte diameter was determined by image analysis using Fiji (ImageJ) with AdipoCorr plugin. Following erythrocyte lysis and serial filtration, stroma-vascular cells were counted and further analyzed by flow cytometry.

Flow Cytometry

A total of 100,000 cells were incubated for 30 minutes at 4 °C with fluorescently labeled antibodies (Table 2) in phosphate-buffered saline (PBS) supplemented with 0.5% bovine serum albumin (BSA) and 2 mmol/L ethylenediaminetetraacetic acid (EDTA). After washing steps, cells were analyzed using FACS Canto II flow cytometer (BD Biosciences). Supervised analyses were performed using FACSDiva Pro software (BD Biosciences) and unsupervised analyses were performed using FlowJo software (BD Biosciences).

Statistical Analysis

Statistical analyses were performed using GraphPad Prism (GraphPad Software). Comparisons between two groups were performed using either 2-tailed paired or unpaired Student *t* tests or multiple *t* tests, as appropriate. Comparisons between more than two groups were performed using 1-way or 2-way ANOVA followed by appropriate post hoc tests. Proportions were compared using exact tests for contingency tables (Fisher's exact test or Fisher-Freeman-Halton exact test). Associations between adipocyte diameter distributions, progenitor-cell subsets, demographic variables, and clinical measures were evaluated using Spearman correlation analyses. Unsupervised clustering and heatmap were performed using ClustVis (https://biit.cs.ut.ee/clustvis/) [15]. Two-sided $P < 0.05$ was considered statistically significant.

Results

Orbital adipocytes are smaller and display a distinct size distribution compared with abdominal adipocytes

We first characterized the morphology of mature adipocytes isolated from orbital adipose tissue and compared it with that of abdominal subcutaneous adipose tissue. Regardless of the fat depot, phase-contrast microscopy of mature adipocytes isolated following collagenase digestion shows morphological features characteristic of white adipocytes with a single large lipid droplet. A marked difference in adipocyte morphology between the 2 depots was observed (Figure 1A) and quantitative image analysis confirmed that orbital adipocytes had a significantly smaller mean diameter than abdominal adipocytes (Figure 1A). Importantly, the difference was not simply a uniform leftward shift in adipocyte size. Principal component analysis based on adipocyte-size distributions clearly indicated that adipocyte morphology constitutes a depot-specific phenotype rather than an isolated difference in mean cell size (PC1, 56.6% of variance) (Figure 1B). The shape of the size-distribution profile also differed qualitatively between depots: abdominal adipocytes followed a curvilinear, unimodal distribution with a single peak at 80–100 µm, whereas orbital adipocytes showed a bimodal distribution, with a first peak at 20–40 µm and a second, smaller peak at 80 µm ($P < 0.001$ vs abdominal). Thus, human orbital adipose tissue exhibits a distinctive mature adipocyte phenotype characterized by smaller adipocytes and a specific distribution of adipocyte sizes compared with classical abdominal subcutaneous adipose tissue.

Adipocyte-size repartition is associated with age and clinical features of Graves' orbitopathy

We next examined whether the distinctive size repartition of orbital adipocytes was associated with demographic and clinical characteristics of TED through a first, unbiased clustering

approach based on adipocyte size repartition and then stratification approach based on clinical parameters. Clustering analysis of adipocyte-size repartition (Figure 2A) highlighted two subgroups designated “low diameters” (n = 17) and “high diameters” (n = 11) (Figure 2). The “high-diameters” subgroup showed a size distribution shifted toward larger adipocytes (peak at 80–100 µm) compared with the “low-diameters” subgroup (peak at 20–40 µm; $P < 0.001$ at the 20, 40 and 100 µm bins). These groups were compared with demographic and clinical parameters, including age, BMI, disease activity, EUGOGO classification, TRAb status, Hertel exophthalmometry and Gorman score. As shown in figure 2B, patients in the “high-diameters” subgroup were significantly older than those in the “low-diameters” subgroup ($P < 0.05$), with no difference in BMI showing that the distinctive orbital adipocyte size profile was not a surrogate for systemic adiposity. Stratification of the GO cohort based on clinical parameters showed a numerically higher proportion of TRAb positivity in the “low-diameters” group (~90% vs ~60%), though this did not reach statistical significance after correction for multiple comparisons ($P = 0.069$); Active GO, EUGOGO grade, TSH ≥ 4 mU/L, Hertel ≥ 23 mm and Gorman score ≥ 2 did not differ significantly between subgroups in this sample size although the “low diameter**s**” group exhibited a tendency to more severe/active TED associated with TSH abnormality was observed.

The proportion of small and large adipocytes associate separately with acute disease severity and with age

Across the whole OAT cohort, the fraction of small (40 µm) adipocytes correlated inversely with age (Spearman $r = -0.454$, $P = 0.013$), while the fraction of larger (100 µm) adipocytes correlated positively with age (Spearman $r = 0.531$, $P = 0.003$), indicating a progressive shift from a hyperplastic to a more hypertrophic adipocyte profile with increasing age. Consistent with the bimodal orbital profile noted above, the two peaks segregated with distinct clinical features. Stratifying the adipocyte size-distribution profile by clinical subgroup showed that

patients with sight-threatening, corticosteroid-treated GO had a size distribution weighted toward smaller adipocytes (peak at 40 μm, $P < 0.05$) relative to patients with moderate/severe, corticosteroid-treated or not disease, who showed a relative shift toward larger adipocytes (peak at 80 μm, $P < 0.001$) (Figure 3). TRAb-positive patients likewise showed a size distribution shifted toward larger adipocytes (80 μm bin) relative to TRAb-negative patients, who were enriched for smaller adipocytes (40 μm bin; both $P < 0.05$). After adjustment for age, multiple regression analysis showed that TED severity was still predictor of the repartition of adipocyte diameters (40, 80 and 100 μm) with sight threatening group remaining significantly associated with lower value of the fraction of adipocytes with 40 μm diameters ($\beta = -0.1713$, $P = 0.0071$) while higher value of 80 μm ($\beta = 0.2274$, $P = 0.0018$) and of 100 μm ($\beta = 0.05054$, $P = 0.0284$) relative to the moderate to severe group. Similarly, after adjustment for age, multiple regression analysis in patients with moderate to severe TED only, showed that TRAb status was still a predictor of the adipocyte repartition with group TRAb+ remaining significantly associated with higher value of the fraction of adipocytes with 40 μm diameters ($\beta = 0.1553$, $P = 0.0108$) while lower value of 80 μm ($\beta = -0,1498$, $P = 0.0284$) and of 100 μm ($\beta = -0.04772$, $P = 0.0418$) relative to the TRAb- group. Therefore, the relative weight of the two orbital adipocyte peaks tracked with distinct clinical features: the smaller-diameter peak was more prominent in patients with more severe sight-threatening disease and positive for autoimmune TRAb antibodies, whereas the larger-diameter peak was more prominent with increasing age, suggesting that the bimodal orbital profile reflects the coexistence of two adipocyte subpopulations shaped by different aspects of disease biology.

The $CD45^{-}CD34^{+}$ cell component is proportionally reduced in OAT relative to abdominal SAT

Because adipose tissue remodeling depends not only on mature adipocytes but also on resident APCs, we next examined the SVF of orbital and abdominal adipose tissue by flow cytometry.

Unsupervised analysis of CD45 and CD34 expression revealed distinct SVF profiles between the 2 adipose depots (Figure 4) with few cell clusters in orbital fat reflecting lower cellular diversity (Figure 4). Principal component analysis of SVF composition nonetheless clearly separated orbital from abdominal samples on this basis (PC1, 77.5% of variance) while total SVF cell yield per gram of tissue did not differ significantly between depots. Supervised analysis (Figure 1B) confirmed that the relative composition of the SVF differed markedly, and in the opposite direction: the $CD45^{+}CD34^{-}$ immune fraction and, notably, the $CD45^{-}CD34^{+}$ progenitor fraction was both significantly higher in abdominal SAT ($P < 0.05$ and $P < 0.0001$, respectively) whereas OAT was significantly enriched for the $CD45^{-}CD34^{-}$ double-negative stromal fraction ($P < 0.0001$) with no depot difference in the minor $CD45^{+}CD34^{+}$ fraction.

The orbital progenitor compartment is selectively enriched in $CD55^{+}$ cells

Within the $CD45^{-}CD34^{+}$ compartment, we separated endothelial ($CD34^{+}CD31^{+}$) from progenitor ($CD34^{+}CD31^{-}$) cells (Figure 5). The progenitor fraction represented a significantly smaller proportion of SVF in OAT than in abdominal SAT ($P < 0.0001$), and orbital progenitors expressed lower CD34 mean fluorescence intensity (MFI) than abdominal progenitors ($P < 0.0001$); the endothelial fraction did not differ between depots by either measure. Differential marker analysis of the progenitor gate showed that CD36 expression per cell was the most strongly reduced marker in orbital versus abdominal progenitors with MSCA1 and CD271 also reduced, while CD55 MFI was increased in orbital progenitors. Expressed as absolute progenitor number per gram of tissue, $CD271^{+}$, $CD36^{+}$ and $MSCA1^{+}$ progenitors were all significantly more abundant in abdominal than orbital tissue ($P < 0.05$ for each), whereas $CD55^{+}$ progenitor number showed a non-significant trend toward higher abundance in OAT.

Therefore, the distinctive orbital progenitor phenotype is characterized by both reduced progenitor abundance and reduced CD34 expression, indicating that orbital APCs differ from their abdominal counterparts not only quantitatively but also phenotypically. Orbital adipose

tissue exhibits selective remodeling of the APC compartment, with relative enrichment of $CD55^+$ cells accompanied by lower representation of the other progenitor subsets examined. This observation identifies CD55 expression as a distinctive feature of the orbital APC compartment.

Unsupervised clustering identifies a CD55-enriched orbital progenitor subgroup associated with proptosis

To determine whether progenitor composition stratifies GO patients clinically, we performed unsupervised clustering of orbital SVF composition, which identified three clusters (Figure 6; cluster 1, n = 10; cluster 2, n = 6; cluster 3, n = 9). Cluster 1 was characterized by a high proportion of $CD45^-CD34^-$ cells and a low proportion of $CD45^-CD34^+CD31^-$ progenitors; cluster 3 showed the inverse pattern, with the highest proportion of $CD45^-CD34^+CD31^-$ progenitors ($P < 0.0001$ vs cluster 1); cluster 2 was distinguished by an expanded $CD45^+CD34^-$ (immune) fraction and older patient age. Clinically, cluster 3 showed the highest proportion of patients with Hertel ≥ 23 mm (~85%, $P = 0.044$), while cluster 2 showed the highest proportion of sight-threatening EUGOGO grading (~65%), though without reaching statistical significance ($P = 0.055$). Among progenitor subsets, $CD55^+$ cells were significantly higher in cluster 3 than cluster 1 ($P < 0.0001$), while $CD36^+$, $CD271^+$ and $MSCA1^+$ proportions did not differ significantly across clusters. These results indicate that the cellular organization of orbital adipose tissue is heterogeneous among individuals and that differences in APC composition and more specifically in immune cells and in CD55+progenitors are associated with distinct clinical phenotypes of GO.

CD55+ APCs are associated with proptosis severity and adipocyte morphology

Consistent with the cluster analysis, $CD55^+$ progenitor abundance (% SVF) increased significantly across Hertel tertiles (1st vs 3rd tertile, $P < 0.05$), whereas $CD36^+$, $CD271^+$ and

MSCA1^{+} subsets showed no significant trend (Figure 7). Therefore, CD55+ progenitor subset is linked with the degree of orbital protrusion. Hertel exophthalmometry provides an anatomical measure of orbital expansion and therefore represents an important clinical correlate of the tissue remodeling process. Correlation analysis across the OAT cohort showed that CD55^{+} progenitor abundance correlated positively with the proportion of large adipocytes (80 μm, r = 0.52; 100 μm, r = 0.33; 120 μm, r = 0.42; 140 μm, r = 0.35) and negatively with the proportion of small adipocytes (20 μm, r = −0.39; 40 μm, r = −0.39). CD36^{+} abundance showed a qualitatively similar but weaker pattern (80 μm, r = 0.30; 20/40 μm, r = −0.33), while CD271^{+} showed weak, inconsistent correlations with adipocyte size. MSCA1^{+} abundance correlated with age (r = 0.45) but not consistently with adipocyte diameter. Together, these data indicate that a CD55-enriched progenitor phenotype, rather than the CD36/MSCA1-defined committed-progenitor phenotype, tracks most closely with orbital adipocyte hypertrophy and proptosis severity. Together, these findings link 3 characteristics of orbital adipose tissue: its distinctive mature adipocyte morphology, its selective APC composition, and its clinical phenotype. In particular, the association between CD55^{+} APC abundance and Hertel score identifies this progenitor phenotype as a candidate cellular correlate of orbital expansion.

Discussion

In this study, we demonstrate that human orbital adipose tissue differs from classical abdominal subcutaneous adipose tissue in both mature adipocyte morphology and APC composition. Orbital adipocytes are smaller and display a distinct distribution of cell sizes. In parallel, orbital fat contains fewer $CD45^{-}CD34^{+}CD31^{-}$ progenitors and these cells express less CD34 than abdominal progenitors. Despite this quantitative reduction, the orbital progenitor compartment is compositionally distinct with relative enrichment of $CD55^{+}$ cells and lower representation of $CD271^{+}$, CD36+, and $MSCA1^{+}$ populations. Importantly, these cellular characteristics are associated with clinical features of GO including proptosis.

Our first major finding is that mature adipocytes in orbital fat are markedly smaller than those in abdominal subcutaneous adipose tissue, in agreement with previous reports [16] [6]. Within the GO cohort, however, adipocyte size was not uniform. Rather, the bimodal distribution of orbital adipocyte size suggests the coexistence of two distinct adipocyte phenotypes that may reflect different aspects of disease biology: a small-adipocyte phenotype associated with disease activity and severity, as observed in patients with sight-threatening disease requiring corticosteroid treatment, as well as with positive TRAb status, and a large-adipocyte phenotype associated with increasing age and negative TRAb status. Interestingly, higher TRAb levels have been associated with disease severity, delayed remission, and a more protracted course of GO. Whether these two ends of the adipocyte-size spectrum represent distinct disease trajectories or different stages of a dynamic remodeling process cannot be determined from our cross-sectional study. Likewise, our findings cannot establish whether changes in adipocyte morphology contribute to disease progression or instead reflect the consequences of the local autoimmune and hormonal milieu. However, one might speculate that the enrichment of small adipocytes in active and more severe TED may reflect either increased adipogenic turnover or ongoing TRAb-driven adipogenic remodeling [2,7] . Conversely, in the absence of TSHR

stimulation by TRAb and with increasing age in patients with moderate to severe and inactive GO, the shift towards bigger adipocytes may be due to progressive adipocyte hypertrophy during the course of Graves' orbitopathy. This pattern implies that adipocyte hypertrophy may potentially represent a more stable or chronic phase of orbital tissue remodelling. The underlying mechanisms remain to be established but the reported enhanced intravascular lipolysis through increased lipoprotein lipase and fatty acid uptake combined with lower adipocyte lipolysis [6] may most probably be contributor of adipocyte hypertrophy.

The second major finding concerns the APC compartment. Given that expansion of adipose tissue can involve recruitment and differentiation of resident progenitors, one might anticipate that the orbital expansion observed in GO would be associated with low number of APCs. The $CD45^{-}CD34^{+}CD31^{-}$ progenitor compartment was indeed smaller in orbital than abdominal adipose tissue from normal weight control donors, in agreement with the dynamic orbital cellular remodeling. In addition, orbital progenitors expressed lower levels of CD34. Interestingly progenitor with low CD34 expression has been reported to give rise to low lipid turnover adipocytes [17] and in agreement, low lipolytic as well as lipogenic activity are characteristics of OAT adipocytes [6]. Among the progenitors that were present, orbital cells in patients with GO expressed lower levels of CD36, MSCA1 and CD271 than their abdominal counterparts, markers that in SAT are associated with adipogenic commitment and lineage-specific niches [13,14], while relative CD55 positivity was increased. The biological significance of this CD55 enrichment remains to be established but as $CD55^{+}$progenitor subset is described as quiescent and multipotent progenitor pool, it may reflect higher intrinsic plasticity capacity of OAT than SAT and may be considered a phenotypic marker of an orbital-enriched APC subset. In addition, the association we observed between $CD55^{+}$ progenitor relative abundance and both adipocyte hypertrophy and proptosis raises the possibility that, in the context of GO and more specifically with increasing age, alteration of the commitment process towards

adipogenic and/or myofibrogenic lineages resulting in the accumulation of immature $CD55^+$ progenitor pool may contribute to or result of adipocyte hypertrophy. This would be an opposing, though conceptually parallel, mechanism to the $CD9^+CD55^-$ progenitor subset recently implicated in metabolic dysfunction in visceral fat of patients with type 2 diabetes in part through the upregulation of adipocyte lipolysis [12] underscoring that alterations in $CD55^+/CD55^-$ progenitor balance, in either direction, can mark pathological adipose remodeling in different disease contexts but both associated with changes in adipocyte function and morphology. Whether the $CD55^+$ progenitor subset we describe is itself a direct target of TSHR/TRAb signaling as it commits to the adipogenic lineage, or instead represents a distinct, upstream route to adipogenesis that operates alongside the fibroblast TSHR pathway characterized in prior work [18,19], is an important question for future functional studies, for example by assessing TSHR expression and TSH/TRAb responsiveness specifically in sorted $CD55^+$ versus $CD55^-$ orbital progenitors. As for adipocyte size repartition, longitudinal studies will be required to determine whether specific APC profiles predict progression, response to treatment, or subsequent orbital remodeling.

These findings should be interpreted in light of several limitations. The present study is cross-sectional and observational and cannot therefore establish temporal or causal relationships. Associations between APC subsets, adipocyte morphology and clinical severity are observed from relatively small subgroup sizes, limiting statistical power and should be considered hypothesis-generating. Progenitor subsets were defined by surface marker expression alone; functional assays (in vitro adipogenic and myofibrogenic differentiation, clonogenic and self-renewal assays) on sorted $CD55^+$ versus other subsets orbital progenitors ($CD36^+$, $MSCA1^+$, $CD271^+$) will be required to establish whether the $CD55^+$ population is directly responsible for adipocyte hypertrophy or is instead a bystander or compensatory population. The abdominal SAT comparator, while a standard reference depot, differs from OAT in embryological origin

and future studies should include additional control depots (e.g., healthy OAT from non-GO subjects) where accessible.

In summary, this study demonstrates that OAT in GO harbors a proportionally smaller but phenotypically distinct progenitor compartment relative to abdominal SAT and that, within this reduced pool, a CD55-enriched, CD36/MSCA1-low progenitor subset is selectively associated with adipocyte hypertrophy and proptosis severity. These findings position $CD55^{+}$ orbital progenitors as a candidate cellular correlate of pathological orbital fat expansion in GO, and nominate this subset for further mechanistic study and evaluation as a biomarker of disease severity and/or relevant target to the pathogenesis and treatment of thyroid eye disease.

Legends of figures

Figure 1. Distinct mature adipocyte morphology and size repartition in orbital and abdominal adipose tissue

A) Representative histological sections and mean adipocyte diameter in orbital (n = 29) versus abdominal (n = 14) adipose tissue (top; ****P < 0.0001). B) Principal component analysis (Bottom left) and profiles of binned adipocyte size distribution (***P < 0.001 at indicated bins) (Bottom right) in orbital (n = 29, blue) versus abdominal (n = 14, dark) adipose tissue.

Figure 2. Unsupervised clustering identifies orbital adipocyte-size phenotypes associated with clinical characteristics of Graves' thyroid eye disease.

A) Heatmap of unsupervised clustering of individual OAT samples by adipocyte diameter distribution highlighting "low-diameter" (n = 17) and "high-diameter" (n = 11) subgroups (top left), with divergent size-distribution profiles (top right, ***P < 0.001). B) Demographic characteristics of the low and high diameter groups (bottom left, *P < 0.05) and clinical characteristics expressed as % of patients for each group with Gorman score ≥ 2, Hertel ≥ 23 mm, TSH ≥ 4 mU/L, TRAb+ (more than 1.7 UI/L), Sight-threatening TED from EUGOGO classification and Active GO (clinical activity score of 5) (Bottom right).

Figure 3. TED severity, TRAb status and age are associated with adipocyte-size distribution

A) Correlation of the small (40 µm) and large (100 µm) adipocyte fractions with age (Spearman correlation). B) Adipocyte-size distributions according to TED severity, including sight-threatening disease (n = 5), moderate/severe disease with (n = 3) and without (n = 20) corticosteroid exposure (*P < 0.05, ***P < 0.001). C) Adipocyte-size distributions according to TRAb status in patients with moderate/severe TED ($TRAb^-$ less than 1.7 UI/L, n = 5; $TRAb^+$ more than 1.7 UI/L, n = 12) (*P < 0.05).

Figure 4. Orbital and abdominal adipose tissues have distinct stromal vascular fraction compositions.

A) Representative t-SNE plots of CD34 and CD45 expression in orbital (n = 10) and abdominal (n = 10) SVF. B) Representative quadrant gating of CD45 versus CD34. C) Principal component analysis of the percentages of CD45 and CD34 cell subsets in orbital (n = 25) and abdominal (n = 10). D) Total SVF yield per gram of orbital (n = 21) and abdominal (n = 10) tissue and relative proportions of the four CD45/CD34-defined populations in orbital (n = 25) and abdominal (n = 10) SVF (*P < 0.05, ****P < 0.0001).

Figure 5. Orbital and abdominal progenitors differ in CD34, CD36, MSCA1, CD271 and CD55 expression.

A) Representative gating of endothelial ($CD34^{+}CD31^{+}$) versus progenitor ($CD34^{+}CD31^{-}$) cells (top) and their relative proportion and CD34. Mean fluorescence intensity (MFI) in orbital (n = 25) versus abdominal (n = 10) SVF (middle, ****P < 0.0001). B) Volcano plot of CD36, MSCA1, CD271 and CD55 marker mean fluorescence intensity (MFI) differences (orbital − abdominal) in progenitors and absolute progenitor subset number per gram of tissue (*P < 0.05).

Figure 6. Unsupervised clustering identifies orbital stromal cellular phenotypes associated with clinical characteristics of Graves' thyroid eye disease.

A) Heatmap of unsupervised clustering of individual samples by percentages of CD45 and CD34 subtypes highlighting three clusters (cluster 1, n = 10; cluster 2 n = 6; cluster 3 n = 9) and repartition of SVF cell-types across three unsupervised clusters (top, *P < 0.05 to ****P < 0.0001). B) Demographic characteristics of the clusters (left, *P < 0.05) and clinical characteristics expressed as % of patients for each cluster with Gorman score ≥ 2, Hertel ≥ 23 mm, TSH ≥ 4 mU/L, TRAb+ (more than 1.7 UI/L), Sight-threatening TED from EUGOGO

classification and active GO (clinical activity score of 5) (right). C) Progenitor subset composition of the clusters (****P < 0.0001) by cluster.

Figure 7. CD55+ progenitor abundance is associated with Hertel score and correlates with adipocyte-size distribution.

A) $CD55^+$, $CD36^+$, $CD271^+$, and $MSCA1^+$ progenitor subset abundance (% SVF) across Hertel exophthalmometry tertiles (*P < 0.05). B) Spearman correlation matrix relating progenitor subset abundance to age, BMI and adipocyte diameter fraction (20–140 μm). Spearman r is indicated for each pair.

References

1 Bahn, R. S. Graves' ophthalmopathy. *N Engl J Med 2010,* **362**, 726-738. https://doi.org:10.1056/NEJMra0905750

2 Draman, M. S., Zhang, L., Dayan, C. & Ludgate, M. Orbital Signaling in Graves' Orbitopathy. *Front Endocrinol (Lausanne) 2021,* **12**, 739994. https://doi.org:10.3389/fendo.2021.739994

3 Rajaii F, Kim DW, Pan J, Mahoney NR, Eberhart CG, Qian J, *et al.* Temperature and species-dependent regulation of browning in retrobulbar fat. *Sci Rep 2021,* **11**, 3094. https://doi.org:10.1038/s41598-021-82672-9

4 Sebo, Z. L. & Rodeheffer, M. S. Assembling the adipose organ: adipocyte lineage segregation and adipogenesis in vivo. *Development 2019,* **146,** dev172098. https://doi.org:10.1242/dev.172098

5 Cheng, Y., Zhang, K., Liu, J. & Liu, G. Is orbital adipose tissue obesity-privileged? The relationship between small adipocyte size and metabolically healthy state from the view of orbital fat. *J Endocrinol Invest 2025,* **48**, 1549-1562. https://doi.org:10.1007/s40618-025-02568-7

6 Zhang L, Evans A, von Ruhland C, Draman MS, Edkins S, Vincent AE, *et al.* Distinctive Features of Orbital Adipose Tissue (OAT) in Graves' Orbitopathy. *Int J Mol Sci* 2020, **21,** 9145. https://doi.org:10.3390/ijms21239145

7 Kim DW, Kim S, Han J, Belday K, Li E, Mahoney N, *et al.* Transcriptomic profiling of thyroid eye disease orbital fat demonstrates differences in adipogenicity and IGF-1R pathway. *JCI Insight* 2024, **9**, *e182352*. https://doi.org:10.1172/jci.insight.182352

8 Sengenes, C., Lolmede, K., Zakaroff-Girard, A., Busse, R. & Bouloumie, A. Preadipocytes in the human subcutaneous adipose tissue display distinct features from

the adult mesenchymal and hematopoietic stem cells. *J Cell Physiol* **205**, 114-122 (2005).

9 Maumus M, Peyrafitte JA, D'Angelo R, Fournier-Wirth C, Bouloumié A, Casteilla L, *et al.* Native human adipose stromal cells: localization, morphology and phenotype. *Int J Obes (Lond)* 2011 ;35 :1141-53. doi: 10.1038/ijo.2010.269.

10 Merrick D, Sakers A, Irgebay Z, Okada C, Calvert C, Morley MP, *et al.* Identification of a mesenchymal progenitor cell hierarchy in adipose tissue. *Science 2019,* **364** 364(6438):eaav2501. https://doi.org:10.1126/science.aav2501

11 Emont MP, Jacobs C, Essene AL, Pant D, Tenen D, Colleluori G, *et al.* A single-cell atlas of human and mouse white adipose tissue. *Nature 2022,* **603**, 926-933. https://doi.org:10.1038/s41586-022-04518-2

12 Wang H, Du Y, Huang S, Sun X, Ye Y, Sun H, *et al.* Single-cell analysis reveals a subpopulation of adipose progenitor cells that impairs glucose homeostasis. *Nat Commun* 2024, **15**, 4827. https://doi.org:10.1038/s41467-024-48914-w

13 Gao H, Volat F, Sandhow L, Galitzky J, Nguyen T, Esteve D, *et al.* CD36 Is a Marker of Human Adipocyte Progenitors with Pronounced Adipogenic and Triglyceride Accumulation Potential. *Stem Cells 2017,* **35**, 1799-1814. https://doi.org:10.1002/stem.2635

14 Estève D, Boulet N, Belles C, Zakaroff-Girard A, Decaunes P, Briot A, *et al.* Lobular architecture of human adipose tissue defines the niche and fate of progenitor cells. *Nat Commun 2019,* **10**, 2549. https://doi.org:10.1038/s41467-019-09992-3

15 Metsalu, T. & Vilo, J. ClustVis: a web tool for visualizing clustering of multivariate data using Principal Component Analysis and heatmap. *Nucleic Acids Res 2015,* **43**, W566-570. https://doi.org:10.1093/nar/gkv468

16 Bujalska IJ, Durrani OM, Abbott J, Onyimba CU, Khosla P, Moosavi AH, *et al.* Characterisation of 11beta-hydroxysteroid dehydrogenase 1 in human orbital adipose tissue: a comparison with subcutaneous and omental fat. *J Endocrinol 2007,* **192**, 279-288. https://doi.org:10.1677/JOE-06-0042

17 Raajendiran A, Ooi G, Bayliss J, O'Brien PE, Schittenhelm RB, Clark AK, *et al.* Identification of Metabolically Distinct Adipocyte Progenitor Cells in Human Adipose Tissues. *Cell Rep 2019,* **27**, 1528-1540e7. https://doi.org:10.1016/j.celrep.2019.04.010

18 Valyasevi RW, Erickson DZ, Harteneck DA, Dutton CM, Heufelder AE, Jyonouchi SC, *et al.* Differentiation of human orbital preadipocyte fibroblasts induces expression of functional thyrotropin receptor. *J Clin Endocrinol Metab 1999,* **84**, 2557-2562. https://doi.org:10.1210/jcem.84.7.5838

19 Valyasevi, R. W., Harteneck, D. A., Dutton, C. M. & Bahn, R. S. Stimulation of adipogenesis, peroxisome proliferator-activated receptor-gamma (PPARgamma), and thyrotropin receptor by PPARgamma agonist in human orbital preadipocyte fibroblasts. *J Clin Endocrinol Metab 2002,* **87**, 2352-2358. https://doi.org:10.1210/jcem.87.5.8472

Figure 1

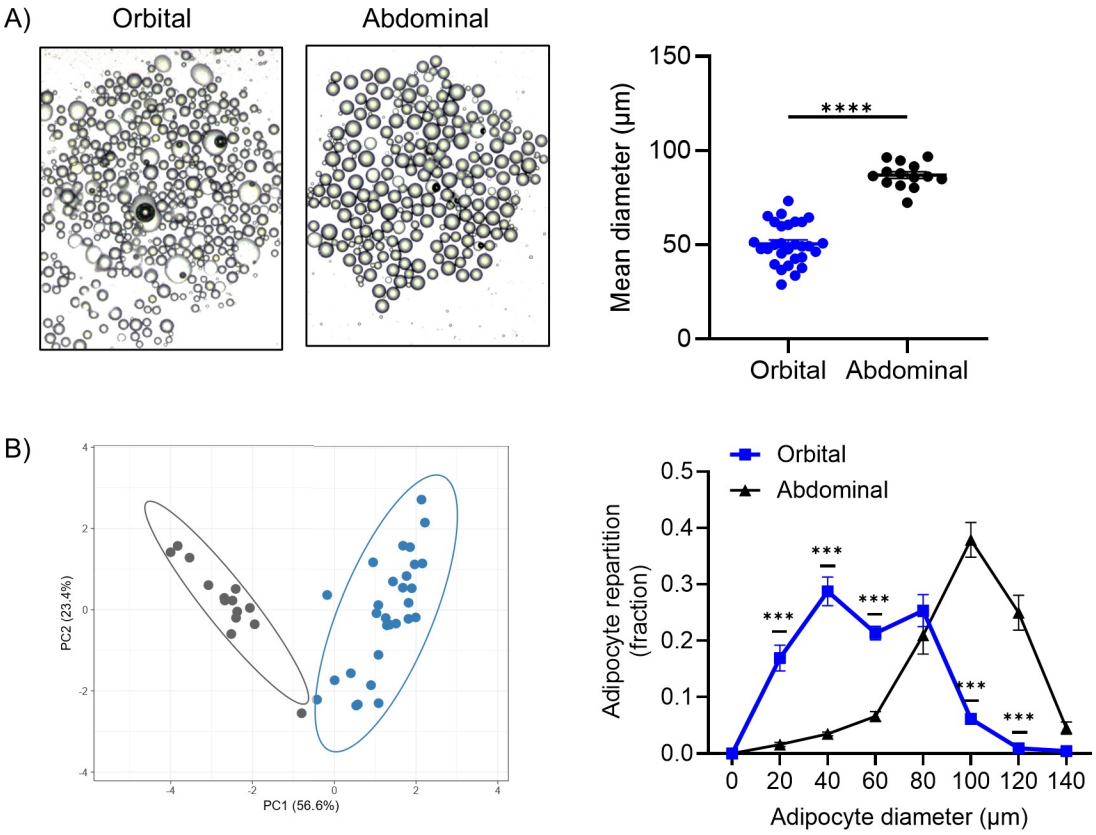

A)
Orbital
Abdominal
Mean diameter (µm)
150
100
50
0
****
Orbital
Abdominal
B)
PC2 (23.4%)
PC1 (56.6%)
Orbital
Abdominal
Adipocyte repartition (fraction)
0.5
0.4
0.3
0.2
0.1
0.0
***
0
20
40
60
80
100
120
140
Adipocyte diameter (µm)

Figure 2

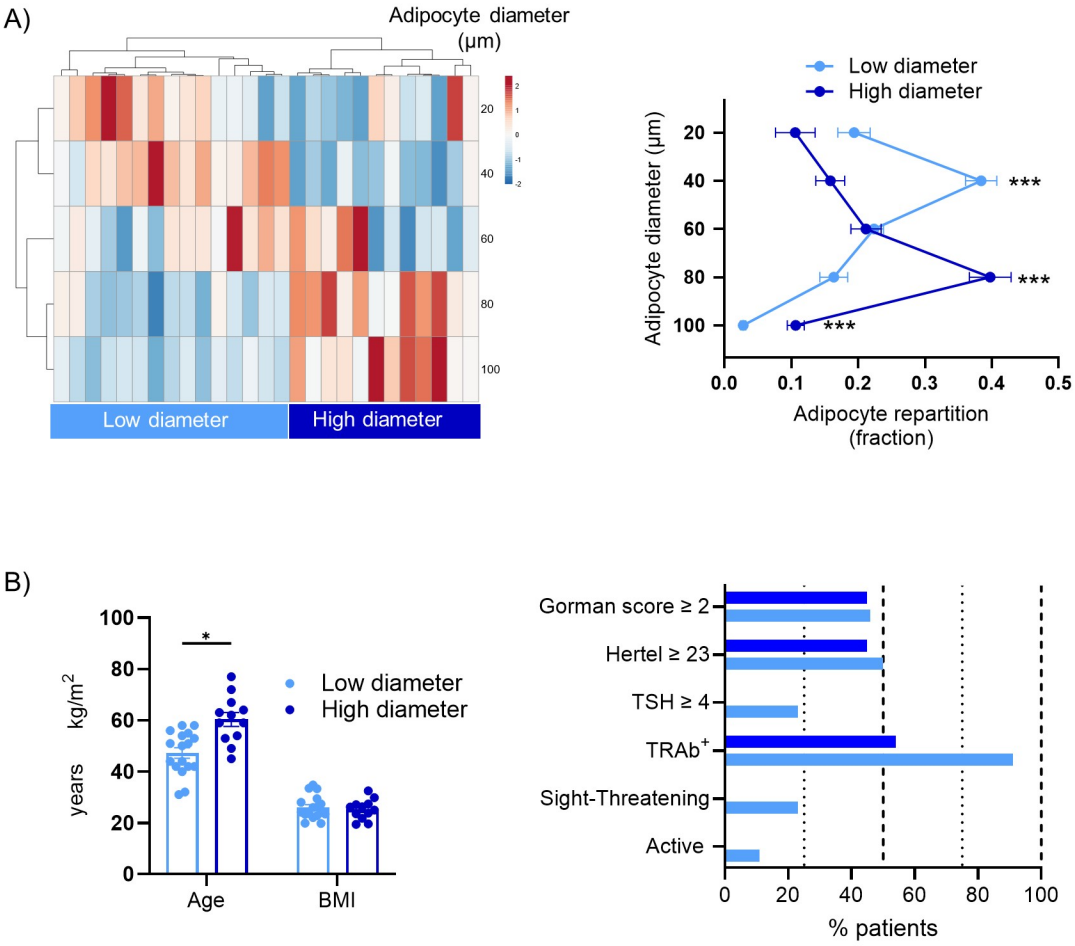

A)
Adipocyte diameter (µm)
20
40
60
80
100
Low diameter
High diameter
Low diameter
High diameter
Adipocyte diameter (µm)
20
40
60
80
100
***
***
***
0.0
0.1
0.2
0.3
0.4
0.5
Adipocyte repartition (fraction)
B)
100
80
60
40
20
0
years kg/m2
*
Low diameter
High diameter
Age
BMI
Gorman score ≥ 2
Hertel ≥ 23
TSH ≥ 4
TRAb+
Sight-Threatening
Active
0
20
40
60
80
100
% patients

Figure 3

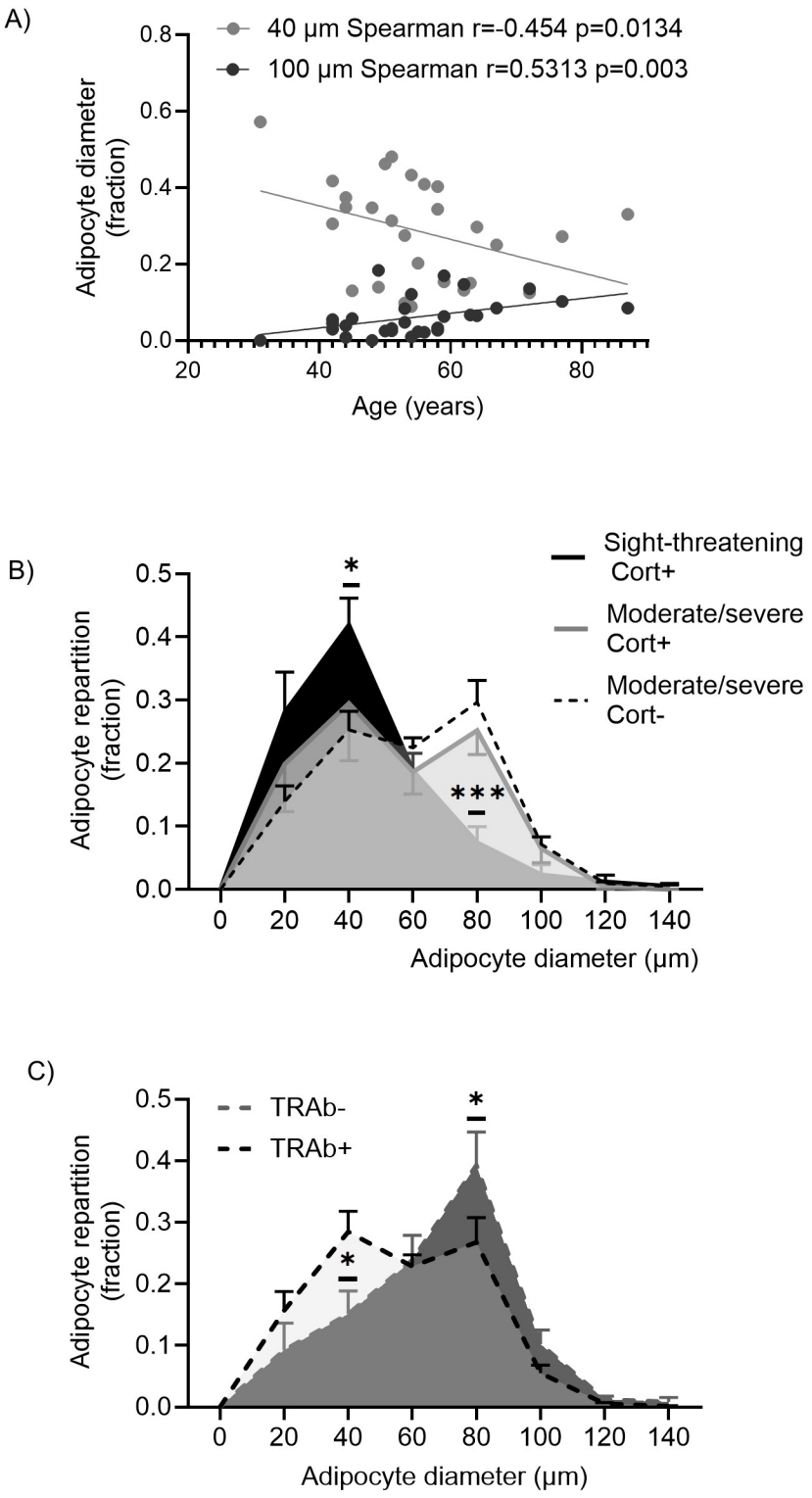

A)
40 µm Spearman r=-0.454 p=0.0134
100 µm Spearman r=0.5313 p=0.003
Adipocyte diameter (fraction)
Age (years)
B)
Sight-threatening Cort+
Moderate/severe Cort+
Moderate/severe Cort-
Adipocyte repartition (fraction)
Adipocyte diameter (µm)
C)
TRAb-
TRAb+
Adipocyte repartition (fraction)
Adipocyte diameter (µm)

Figure 4

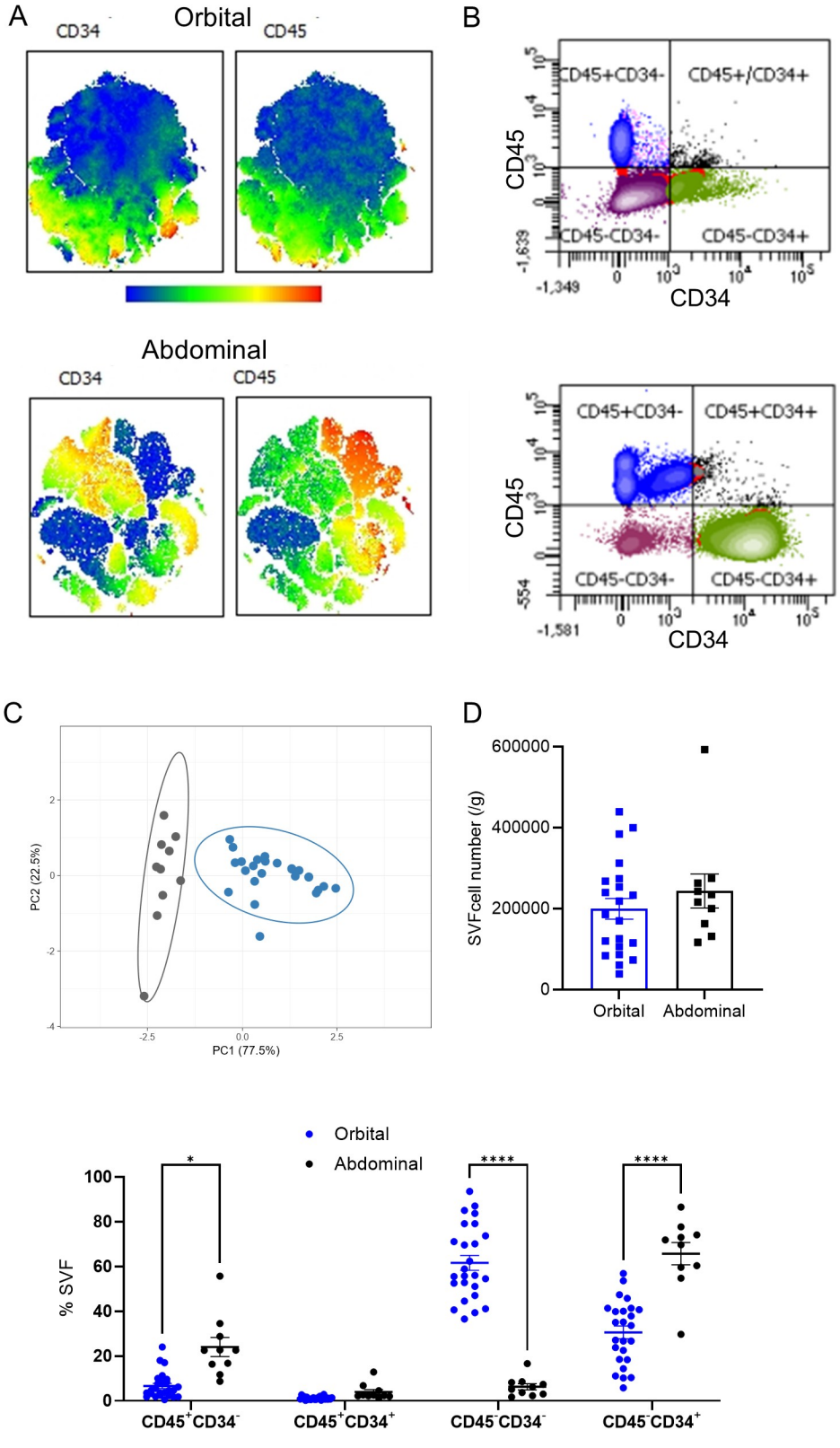

A
Orbital
CD34
CD45
Abdominal
CD34
CD45
B
CD45+CD34-
CD45+/CD34+
CD45-CD34-
CD45-CD34+
CD45
CD34
-1,639
-1,349
CD45+CD34-
CD45+CD34+
CD45-CD34-
CD45-CD34+
CD45
CD34
-554
-1,581
C
PC2 (22.5%)
PC1 (77.5%)
D
SVFcell number (/g)
600000
400000
200000
0
Orbital
Abdominal
Orbital
Abdominal
% SVF
100
80
60
40
20
0
*
****
****
CD45+CD34-
CD45+CD34+
CD45-CD34-
CD45-CD34+

Figure 5

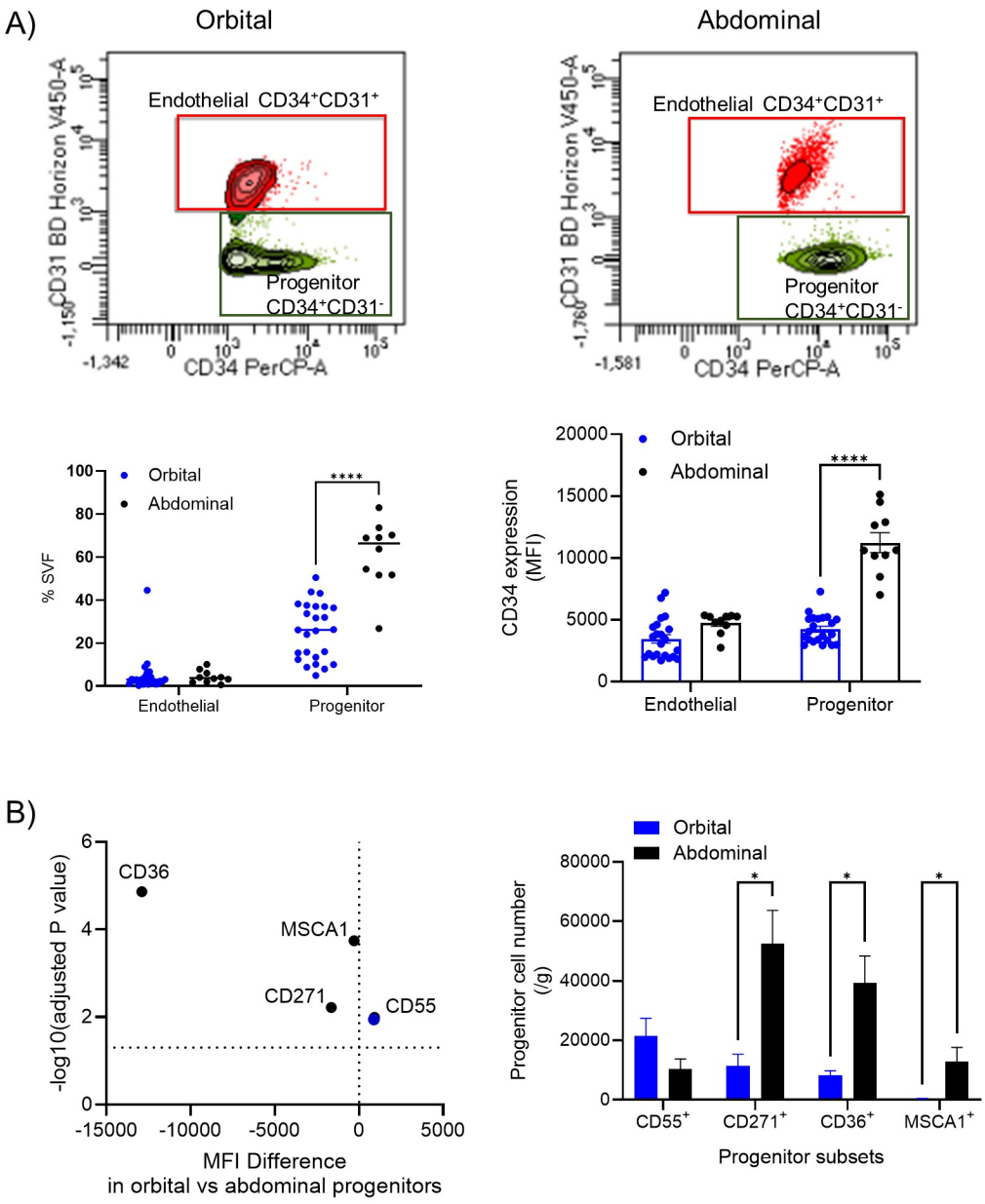

A)
Orbital
Abdominal
Endothelial CD34+CD31+
Progenitor CD34+CD31-
CD31 BD Horizon V450-A
CD34 PerCP-A
% SVF
Orbital
Abdominal
****
Endothelial
Progenitor
CD34 expression (MFI)
B)
CD36
MSCA1
CD271
CD55
-log10(adjusted P value)
MFI Difference in orbital vs abdominal progenitors
Progenitor cell number (/g)
CD55+
CD271+
CD36+
MSCA1+
Progenitor subsets

Figure 6

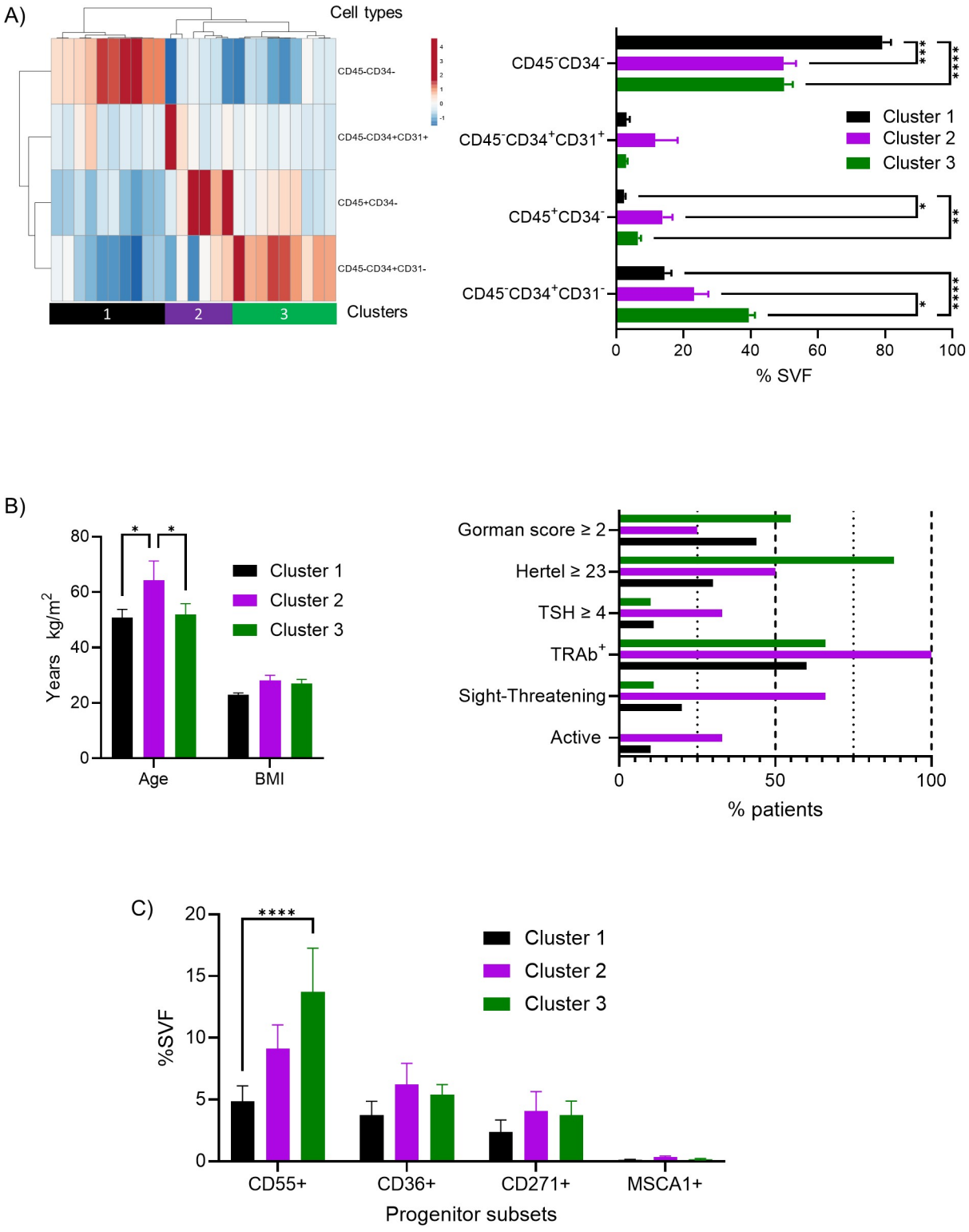
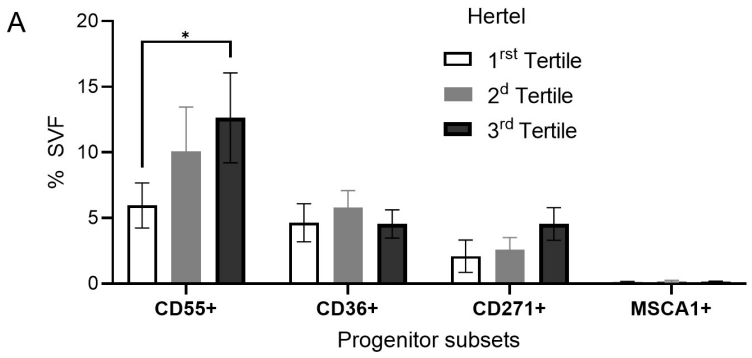
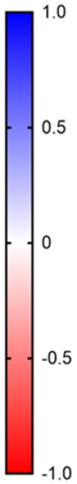

A)
Cell types
CD45-CD34-
CD45-CD34+CD31+
CD45+CD34-
CD45-CD34+CD31-
1
2
3
Clusters
CD45⁻CD34⁻
CD45⁻CD34⁺CD31⁺
CD45⁺CD34⁻
CD45⁻CD34⁺CD31⁻
Cluster 1
Cluster 2
Cluster 3
0
20
40
60
80
100
% SVF
B)
Years kg/m²
Age
BMI
Gorman score ≥ 2
Hertel ≥ 23
TSH ≥ 4
TRAb⁺
Sight-Threatening
Active
% patients
C)
%SVF
CD55+
CD36+
CD271+
MSCA1+
Progenitor subsets

Figure 7



B

Progenitor subsets		CD55+	CD36+	CD271+	MSCA1+
	Age	0.04	0.04	0.04	0.45
	BMI	0.35	0.03	0.27	0.08
Adipocyte diameter (µm)	20	-0.39	-0.33	-0.06	0.42
	40	-0.39	-0.33	0.24	0.05
	60	0.10	0.21	0.33	-0.24
	80	0.52	0.30	-0.13	-0.09
	100	0.33	0.30	-0.23	-0.05
	120	0.42	0.25	-0.27	0.16
	140	0.35	0.15	-0.05	-0.07



Supplementary Files

This is a list of supplementary files associated with this preprint. Click to download.

- Table1pdf.pdf
- Table2pdf.pdf